Title

Influence of Miscibility on Poly(ethylene oxide) Crystallization from Disordered Melts of Block Copolymers with Lithium and Magnesium Counterions

Journal

Macromolecules, 50(12)

ISSN

0024-9297

Authors

Thelen, Jacob L
Chen, X Chelsea
Inceoglu, Sebnem
et al.

Publication Date

2017-06-27

DOI

10.1021/acs.macromol.7b00735

Peer reviewed

Macromolecules

Article

pubs.acs.org/Macromolecules

Influence of Miscibility on Poly(ethylene oxide) Crystallization from Disordered Melts of Block Copolymers with Lithium and Magnesium Counterions

Jacob L. Thelen,[†,‡,§] X. Chelsea Chen,[‡] Sebnem Inceoglu,[‡,§] and Nitash P. Balsara*[,†,‡,§,∥]

[†]Department of Chemical and Biomolecular Engineering, University of California, Berkeley, Berkeley, California 94720, United States
[‡]Materials Sciences Division, [§]Joint Center for Energy Storage Research (JCESR), and [∥]Environmental Energy Technologies Division, Lawrence Berkeley National Laboratory, Berkeley, California 94720, United States

Supporting Information

ABSTRACT: Crystallization within block copolymers is a subject of considerable interest; however, little is understood about how the presence of an ion-containing block, such as poly[(styrene-4-sulfonyltrifluoromethylsulfonyl)imide (P[(STFSI)]), influences the crystallization behavior of single-ion conducting block copolymers derived from poly(ethylene oxide)-*b*-poly[(styrene-4-sulfonyltrifluoromethylsulfonyl)imide (PEO−P[(STFSI)]). In this study, we report on the crystallization behavior of PEO in a matched-set library of lithiated (PEO−P[(STFSI)Li]) and magnesiated (PEO−P[(STFSI)$_2$Mg]) single-ion conducting block copolymers that are disordered in the melt. Structural and thermal analysis of semicrystalline samples prepared by quenching amorphous melts reveals that total PEO crystallinity is independent of cation identity. Furthermore, crystallization induces the formation of lamellar nanostructures regardless of the counterion present. However, the quality of the PEO crystallites and concomitant nanostructures appears to be strongly influenced by counterion identity; magnesiated samples demonstrate more disorder at both the crystalline and nanostructural level. By monitoring PEO crystallization with *in situ* small and wide-angle X-ray scattering, we show that PEO crystallizes from a homogeneous melt within PEO−P[(STFSI)Li] but is hindered by the presence of disordered concentration fluctuations within the magnesiated samples. Thus, counterion identity influences PEO crystallization by controlling the miscibility of the polymer blocks within the crystallizing melt.

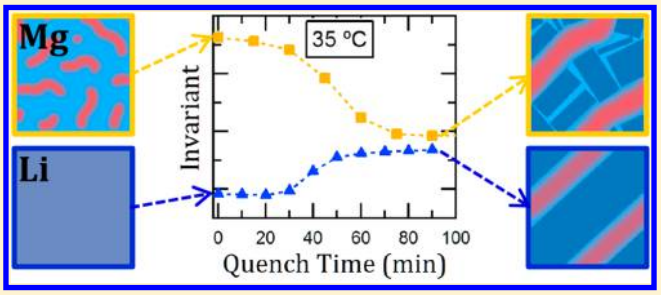

INTRODUCTION

Single-ion conducting block copolymers have recently garnered considerable interest for their potential application in high energy lithium metal batteries.[1−4] A promising class of single-ion conducting block copolymers comprise the ion-containing polymer poly(styrene-4-sulfonyltrifluoromethylsulfonyl)imide lithium (P[(STFSI)Li]) and the ion-conducting polymer poly(ethylene oxide) (PEO).[2] Recently we reported on ion transport in a library of single-ion conducting diblock copolymers of PEO-*b*-P[STFSI], with both lithium and magnesium counterions.[5] The chemical structures of the block copolymers are shown in Figure 1. A major finding in that work was that counterion dissociation from the P[STFSI] backbone could induce mixing of the PEO and P(STFSI) blocks; consequently, the melt morphology and ionic conductivity were strongly coupled. For example, lithium ions were found to readily dissociate from the P[STFSI] block to coordinate with PEO, leading to high ionic conductivity and strong mixing between the PEO and P[STFSI] blocks. In contrast, the lack of dissociation of magnesium counterions from the P[STFSI] block led to poor conductivity and strong concentration fluctuations in the disordered melt. In this work, we study the influence of the lithiated and magnesiated P[STFSI] blocks on the crystallization of PEO within PEO-*b*-P[STFSI] single-ion conducting block copolymers.

Crystallization in neutral block copolymers has been well-studied and is known to both induce and be influenced by nanostructuring.[6−13] In the case of microphase-separated block copolymers, polymer crystallization can either be confined within the nanoscale microphases or the crystallites may "break out" from the microphases and destroy the self-assembled nanostructure of the polymer.[6,7,10−13] For block copolymers that are disordered in the melt, polymer crystallization can effectively induce periodic nanostructural order.[7−9] Crystallization-induced nanostructures have previously been demonstrated in PEO−P[(STFSI)Li] diblock copolymers.[3,4] Since the lithiated (PEO−P[(STFSI)Li]) and the magnesiated (PEO−P[(STFSI)$_2$Mg]) single-ion conducting block copolymers in the present study (see Figure 1) have disordered melt

Received: April 8, 2017
Revised: June 3, 2017
Published: June 15, 2017

DOI: 10.1021/acs.macromol.7b00735
Macromolecules 2017, 50, 4827−4839

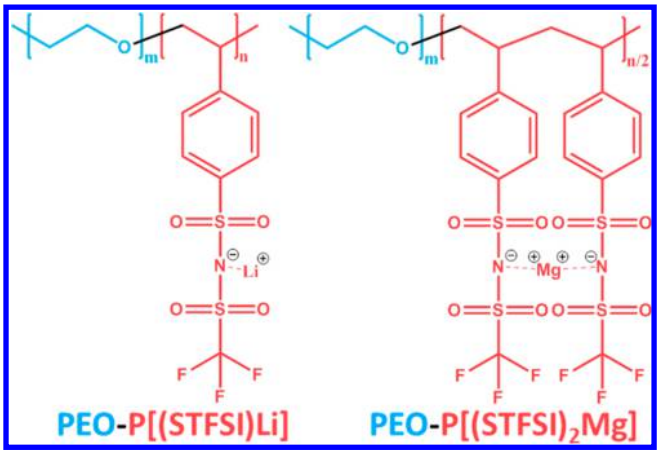

Figure 1. Chemical structures for both types of single-ion block copolymers characterized in this study.

morphologies,[5] we also expect to observe crystallization-induced self-assembly.

The main difference between our system and all previous studies on block copolymer crystallization (e.g., refs 6–13 from the previous paragraph) is the presence of ionic moieties in the noncrystalline block. In PEO/salt mixtures, the addition of moderate amounts of salt reduces PEO crystallinity and decreases crystallization temperature.[14−17] This is due to interactions between the cation and ether oxygens along the PEO backbone. There is no added salt in our system: interactions between cations and ether oxygens can only occur if the cations dissociate away from the P[STFSI] backbone. In the melt, we have found that cation dissociation dictates the degree of block mixing within the disordered state.[5] Thus, cation dissociation in single-ion conducting block copolymers could influence PEO crystallization directly, through interactions with the ether oxygens or, indirectly, by influencing the morphology of the sample during crystallization.

In this work, we use differential scanning calorimetry (DSC) and wide-angle X-ray scattering (WAXS) analysis to reveal that the degree of cation dissociation in PEO-*b*-P[STFSI] has little impact on total PEO crystallinity if the magnesiated and lithiated samples are exposed to the same thermal history. However, small-angle X-ray scattering (SAXS) and scanning transmission electron microscopy (STEM) results from samples subjected to the same thermal treatment demonstrate that cation identity does influence the nature of the crystallization-induced morphologies seen in PEO-*b*-P[STFSI]. Through *in situ* SAXS/WAXS crystallization experiments, we show that cation identity also influences the kinetics of PEO crystal formation. The differences in crystallization kinetics and crystallization-induced nanostructures stem from the differences in miscibility of PEO and P[STFSI] in the melt: PEO crystallization within the well-mixed PEO−P[(STFSI)Li] samples occurs in a manner similar to homopolymer PEO, whereas the presence of strong concentration fluctuations within the PEO−P[$(STFSI)_2$Mg] samples slow down PEO crystallization kinetics and inhibit the formation of well-ordered crystallization-induced nanostructures.

EXPERIMENTAL SECTION

Materials. The synthesis and characterization of the single-ion conducting block copolymer library was described previously.[5] After synthesis, PEO−P[(STFSI)Li] and PEO−P[$(STFSI)_2$Mg] samples were dried under vacuum for a minimum of 1 week at ambient temperature and then dried under vacuum in a heated glovebox antechamber at 90 °C for 24 h before being brought into an argon (Ar) glovebox (MBraun). Inert atmosphere was maintained for all subsequent sample preparation and analysis. We provide the chemical structures of the lithiated and magnesiated versions of the single-ion conducting block copolymer in Figure 1 as well as the chain characteristics of each sample in Table 1.

Thermal Analysis. We previously reported on the thermal characterization of the PEO(5), PEO−P[(STFSI)Li], and PEO−P[$(STFSI)_2$Mg] samples as measured with differential scanning calorimetry (DSC).[5] In this work, we expand upon our analysis of that data in order to explore the crystallization behavior of PEO. For convenience, we summarize the methodology used here and provide the data and analysis details in the Supporting Information (SI 1). The DSC samples were prepared in an Ar glovebox by placing 6−8 mg of polymer into a TZero aluminum pan and sealing with a TZero hermetic lid (T.A. Inc.). A reference TZero hermetically sealed pan was also prepared in the Ar glovebox. In order to ensure the polymers had consistent thermal history, the hermetically sealed DSC samples (and reference pan) were subsequently annealed at 135 °C in a vacuum oven at −10 mmHg for 24 h, after which the heater was turned off and the samples were allowed to slowly cool. Measurements were performed a minimum of 72 h after the oven heater was turned off. A heat−quench−heat−cool method was used in order to determine the melting temperature (T_m) and fractional crystallinity (x_{cr}^{DSC}), crystallization temperature (T_c), and in cases where observable glass transition temperature (T_g) of PEO.[5]

Small- and Wide-Angle X-ray Scattering (SAXS/WAXS). The details involving scattering sample preparation and data collection have been described previously.[5] In brief, all SAXS/WAXS samples, including an empty reference cell, were prepared inside of an Ar glovebox. The polymer samples were made by melt-forming into a custom-built hermetically sealed sample holder with 25 μm Kapton film windows. The samples were subsequently removed from the glovebox and thermally pretreated using the protocol described above for the DSC samples.

The SAXS/WAXS experiments were performed at Lawrence Berkeley National Laboratory's Advanced Light Source, Beamline 7.3.3,[18] using a transmission setup and a custom-built heating stage. Temperature scans were replicated using both SAXS and WAXS. For each experiment, the samples were initially equilibrated at near ambient conditions (either 30 or 35 °C) where the scattering of

Table 1. Characteristics of the Matched Set of Block Copolymers[a]

sample name	$M_{n,PEO}$ [kg mol^{-1}]	$M_{n,P(STFSI)}$ [kg mol^{-1}]	N_{PEO}	N_{PSTFSI}	ϕ_{PEO}
PEO-P[(STFSI)Li](5-3.2)	5.00	3.19	114	9.9	0.68
PEO-P[(STFSI)Li](5-2.0)	5.00	1.99	114	6.2	0.76
PEO−P[(STFSI)Li](5-1.1)	5.00	1.05	114	3.3	0.84
PEO−P[$(STFSI)_2$Mg]{5-3.2)	5.00	3.24	114	9.9	0.67
PEO−P[$(STFSI)_2$Mg](5-2.0)	5.00	2.02	114	6.2	0.76
PEO−P[$(STFSI)_2$Mg](5-1.1)	5.00	1.08	114	3.3	0.84
PEO(5)	5.00		114		1

[a] N_{PEO} and N_{PSTFSI} are the number-average degrees of polymerization for each block, and ϕ_{PEO} is the volume fraction of PEO.

DOI: 10.1021/acs.macromol.7b00735
Macromolecules 2017, 50, 4827−4839

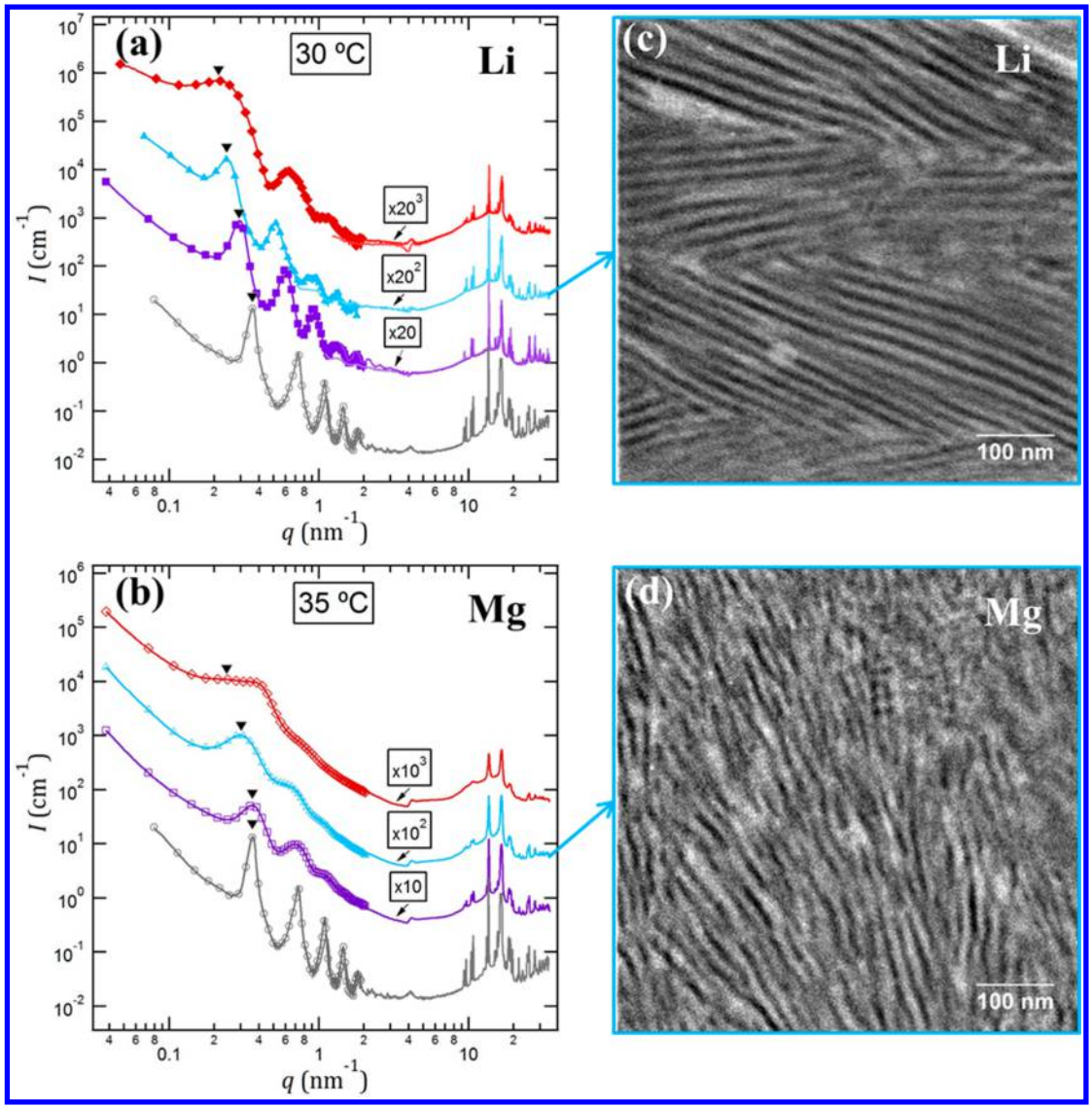

Figure 2. (a, b) Combined SAXS/WAXS profiles where scattering intensity, I, is plotted versus the magnitude of the scattering vector, q, for (a) the lithiated (PEO−P[(STFSI)Li]) (closed symbols) and (b) magnesiated (PEO−P[$(STFSI)_2Mg$]) (open symbols) samples at ambient conditions after thermal pretreatment. P(STFSI) chain length decreases from top to bottom in each plot, with the red diamonds/curves = PEO−P(STFSI)(5-3.2); cyan triangles/curves = PEO−P(STFSI)(5-2.0); purple squares/curves = PEO−P(STFSI)(5−1.1); and for reference, the scattering from PEO(5) is provided in open gray circles/curves. For clarity, SAXS data markers are only plotted for every 15th data point, WAXS data are represented by lines between data points, and the absolute intensity profiles are offset by the factors indicated on the plot. The locations of the primary scattering peaks are marked with black upside-down triangles. The feature in the scattering data near q = 4 nm^{-1} is due to imperfect subtraction of the scattering from the Kapton sample holder windows. (c, d) STEM micrographs from thermally pretreated, cryo-microtomed, and stained samples of (c) PEO−P[(STFSI)Li](5-2.0) and (d) PEO−P[$(STFSI)_2Mg$](5-2.0). The bright phase indicates PEO-rich regions.

semicrystalline samples was recorded. The samples were then heated directly to 130 °C and held at that temperature for at least 1 h. The stage was subsequently cooled in 20 °C steps down to 90 or 70 °C. Measurements were performed at each temperature upon waiting at least 30 min after the stage reached the target set point. Finally, in cases when beamtime was available, the samples were quenched directly to 35 °C and allowed to isothermally crystallize for at least 90 min (note, the stage took ∼45 min to reach 35 °C), with scattering patterns being measured every 10−15 min. As noted previously, the actual sample temperature was found to be approximately 0.94 times the stage set point.[5] We report all temperatures as the set point temperature for simplicity.

The 2D scatting images were reduced using the Nika macro developed by Jan Ilavsky[19] in Igor Pro, as detailed in the Supporting Information (SI 2). The resulting 1D data from both SAXS and WAXS were further corrected for sample transmission and parasitic scattering from the sample holder and were calibrated to absolute intensity units using a glassy carbon (GC) standard provided by Jan Ilavsky (Sample M13).[20] Details of the data corrections, including a detailed derivation of an improved angle-dependent absorption correction for the WAXS data, can be found in the Supporting Information (SI 3). All corrected 1D combined SAXS/WAXS scattering profiles from the temperature scan of the thermally pretreated samples as well as the 1D scattering profiles from the *in situ* isothermal (35 °C) crystallization experiments are included in SI 5.

Scanning Transmission Electron Microscopy (STEM). STEM measurements were performed on two of the semicrystalline ion-containing block copolymers: PEO−P[(STFSI)Li](5-2.0) and PEO−P[$(STFSI)_2Mg$](5-2.0). These samples underwent the same thermal treatment as the DSC and SAXS/WAXS samples. The thermally pretreated samples were cryo-microtomed at −90 °C in a Leica FC6. Sections with thickness approximately 100 nm were obtained using a

DOI: 10.1021/acs.macromol.7b00735
Macromolecules 2017, 50, 4827−4839

Table 2. Thermal and Structural Polymer Properties

Sample Name	Thermal Analysis (DSC)					Structural Analysis (WAXS)			
	T_m [°C]	T_c [°C]	ΔH_m [Jg^{-1}]	x_{cr}^{DSC}	ϕ_{cr}^{DSC}	ϕ_{cr}^{WAXS}	$I_{p,[120]}$ [cm^{-1}]	$q_{p,[120]}$ [nm^{-1}]	$FWHM_{[120]}$ [nm^{-1}]
PEO-P[(STFSI)Li](5-3.2)	55.7	--	72.5	0.60	0.58	0.59[a] 0.55[b]	1.50[b]	13.758[b]	0.117[b]
PEO-P[(STFSI)Li](5-2.0)	57.9	35.7	101	0.73	0.70	0.70[a] 0.67[b]	2.91[b]	13.741[b]	0.107[b]
PEO-P[(STFSI)Li](5-1.1)	58.1	35.3	121	0.76	0.74	0.78[a] 0.75[b]	2.48[b]	13.729[b]	0.107[b]
PEO-P[(STFSI)$_2$Mg](5-3.2)	57.2	-28.5	71.9	0.60	0.58	0.52	0.46	13.712	0.416
PEO-P[(STFSI)$_2$Mg](5-2.0)	57.2	17.2	100	0.72	0.70	0.64	0.76	13.689	0.265
PEO-P[(STFSI)$_2$Mg](5-1.1)	57.9	23.9	119	0.75	0.72	0.65	1.21	13.687	0.193
PEO(5)	59.8	42.2	175	0.85	0.83	0.79[a] 0.80[b]	2.51[b]	13.637[b]	0.107[b]

[a]Value from the blue-highlighted sector averages in Figures S15, S17, S19, and S21. [b]Value from the pink-highlighted sector averages in Figures S15, S17, S19, and S21.

diamond knife and picked up onto lacey carbon-coated copper grids (Electron Microscopy Sciences). STEM samples were stained in ruthenium tetroxide vapor for 30 min prior to experiments. STEM experiments were performed on an FEI Titan microscope operated at 200 kV at the National Center for Electron Microscopy of the Molecular Foundry, Lawrence Berkeley National Lab. The microscope is equipped with a high angle annular dark field detector (HAADF).

RESULTS AND DISCUSSION

In Figure 2, we provide the combined SAXS/WAXS profiles for all of the lithiated and magnesiated single-ion conducting block copolymers, as well as PEO(5), at ambient temperature after the thermal pretreatment described in the Experimental Section. In general, the SAXS profiles (Figure 2a,b) of the block copolymer samples exhibit the same features as that of the homopolymer PEO(5) sample, i.e., integer-spaced peaks indicative of a stacked lamellar nanostructure. We confirm the presence of lamellar order in PEO−P[(STFSI)Li](5-2.0) and PEO−P[(STFSI)$_2$Mg](5-2.0) with STEM in Figure 2c,d. The location of the primary scattering peak (q^*), which reflects the long period of the stacked lamellar lattice, is indicated by the black upside-down triangles in Figure 2a,b. The methodology used to determine the peak locations is described in the Supporting Information (SI 4). Each of the block copolymer WAXS profiles in Figure 2a,b exhibits Bragg scattering peaks in the same locations as those observed for PEO(5), indicating the presence of crystalline PEO domains; the scattering from PEO(5) is consistent with previous observation.[21] Since neither the Bragg peaks in WAXS nor the integer-spaced SAXS peaks are present for any sample at temperatures above the melting point of PEO (see SI 5), we conclude that the ordered nanostructures observed at ambient temperatures are induced by PEO crystallization. Thus, PEO crystallization and polymer nanostructure are coupled in these samples.

In order to characterize the coupling between PEO crystallization and block copolymer nanostructure, we must first determine the PEO crystallinity for each sample. In this work, we calculate PEO crystallinity using both thermal (DSC) and structural (WAXS) analysis. The crystallinity of PEO determined from DSC (x_{cr}^{DSC}), defined as the mass fraction of crystalline PEO relative to the total mass of PEO within the sample, was calculated using eq 1

$$x_{cr}^{DSC} = \frac{\Delta H_m}{w_{PEO}\Delta H_m^\circ} \quad (1)$$

where ΔH_m is the experimental melting enthalpy, w_{PEO} is the weight fraction of PEO within the sample, and ΔH_m° is the ideal melting enthalpy from a fully crystalline sample. We assume that the ideal melting enthalpy of fully crystalline PEO is ΔH_m° = 206 J g^{-1}.[22] Literature values of ΔH_m° range from 198 to 216 J g^{-1}.[22−24] The x_{cr}^{DSC} values as well as the PEO melting (T_m) and crystallization (T_c) temperatures determined from DSC for all of the samples are provided in Table 2. The DSC data used to obtain these results are shown in Figures S1−S3 of the Supporting Information.

The crystallinity of PEO calculated by WAXS analysis (ϕ_{cr}^{WAXS}) represents the volume of PEO crystals relative to the total volume of PEO within the sample. The presence of the additional amorphous material (i.e., P(STFSI)) in the block copolymer samples complicates the calculation of PEO crystallinity using of typical scattering analysis techniques;[25,26] however, we have developed a framework to extract the crystallinity of PEO using absolute WAXS data, such as that shown in Figure 2a,b. A detailed derivation of our method is provided in the Supporting Information (SI 3). In brief, we have extended the approximation that was proposed by Goppel,[27] and recently employed by Balko and co-workers,[28] to allow for the analysis of block copolymers with one crystallizable block. The Goppel approximation is based on the measurement of the scattering intensity due to the amorphous fraction of a crystallizable polymer in both the semicrystalline (I_{scr}) and fully molten (I_{molten}) state. Through a molar balance it can be shown that the amorphous volume fraction of a semicrystalline sample (ϕ_{am}^{scr}), and hence crystalline volume fraction (ϕ_{cr}^{WAXS}), can be given by

$$\phi_{am}^{scr} \approx \frac{I_{scr}(q_0)}{I_{molten}(q_0)} = 1 - \phi_{cr}^{WAXS} \quad (2)$$

where q_0 is the scattering vector chosen to evaluate I_{scr} and I_{molten}. For eq 2 to provide an accurate measure of crystallinity, the intensity contributions from incoherent scattering and diffuse scattering from crystalline disorder must be negligible compared to the contribution from amorphous polymer at q_0.[27,28] We note that errors induced by incoherent and diffuse

DOI: 10.1021/acs.macromol.7b00735
Macromolecules 2017, 50, 4827−4839

scattering will depress the values of ϕ_{cr}^{WAXS}; thus, the Goppel approximation can be considered a lower bound of the crystalline fraction. The values of ϕ_{cr}^{WAXS} determined from the data in Figure 2a,b are provided in Table 2. For convenience, Table 2 also includes the DSC crystallinity converted to volumetric terms (x_{cr}^{DSC}) by

$$\phi_{cr}^{DSC} = \frac{(x_{cr}^{DSC}/\rho_{cr}^{PEO})}{(x_{cr}^{DSC}/\rho_{cr}^{PEO}) + ((1 - x_{cr}^{DSC})/\rho_{am}^{PEO})} \quad (3)$$

where ρ_{cr}^{PEO} = 1.24 g cm^{-3} is the density of crystalline PEO and ρ_{am}^{PEO} = 1.12 g cm^{-3} is the density of amorphous PEO near ambient temperature.[27]

Inspection of the crystallinity values determined by thermal (DSC) and structural (WAXS) analysis in Table 2 reveals interesting phenomena: both techniques show that PEO crystallinity is reduced by increasing the length of the P(STFSI) block. However, DSC suggests that PEO crystallinity is unaffected by the counterion identity, whereas WAXS shows a small but distinct difference in PEO crystallinity between matched pairs: the magnesiated samples have a lower PEO crystallinity than their lithiated counterparts. PEO crystallinity values determined from DSC and WAXS of all samples are shown in Figure 3a, where ϕ_{cr}^{WAXS} is plotted versus ϕ_{cr}^{DSC}. It is clear from Figure 3a that ϕ_{cr}^{WAXS} and ϕ_{cr}^{DSC} are essentially equivalent (within ±5%) for the lithiated samples as well as for PEO(5); however, the magnesiated samples have ϕ_{cr}^{WAXS} values that are systematically lower than ϕ_{cr}^{DSC} by approximately 7%, as indicated by the linear fit with slope fixed to unity. As noted above, the ϕ_{cr}^{WAXS} values determined using the Goppel approximation can be influenced diffuse scattering from crystalline disorder. Since crystalline disorder should affect the Bragg scattering peaks,[29] we have characterized the changes in PEO crystallites by fitting the PEO [120] peak in each WAXS profile with a simple Gaussian function (SI 4) and provided the resulting peak height ($I_{p,[120]}$), peak position ($q_{p,[120]}$) and full width at half-maximum (fwhm$_{[120]}$) for each sample in Table 2. In Figure 3b, we show the influence of P(STFSI) chain length and counterion identity on PEO crystal disorder by plotting fwhm$_{[120]}$ versus the volume fraction of P(STFSI) (ϕ_{PSTFSI}) for all of the samples. Interestingly, the fwhm$_{[120]}$ values for the lithiated samples are independent of ϕ_{PSTFSI}, while the fwhm$_{[120]}$ values for the magnesiated samples increase significantly with increasing ϕ_{PSTFSI}, following what appears to be a quadratic relation. At this time it remains unclear whether the [120] peak broadening is due to crystallite size or imperfections in the crystalline lattice.[29] The data in Figure 3 indicate that the counterion influences the structure of the PEO crystallites within these PEO–P(STFSI) block copolymers.

In addition to the total crystallinity being unaffected by counterion identity, the melting temperature of the PEO crystals is a weak function of the length of the ion-containing block and the identity of the cation. As shown in Table 2, melting temperatures (T_m's) between 55 and 60 °C are observed in all cases. In PEO homopolymers, single crystals with once- or twice-folded PEO chains exhibit melting temperatures between 57 and 60 °C.[30,31] Nearly all of the samples in the present study have T_m's within that range, suggesting the predominant presence of PEO crystallites with once- and twice-folded chains. The exception lies in PEO–P[(STFSI)Li](5-3.2), where the slightly depressed melting T_m suggests the presence of some kinetically trapped thrice-folded

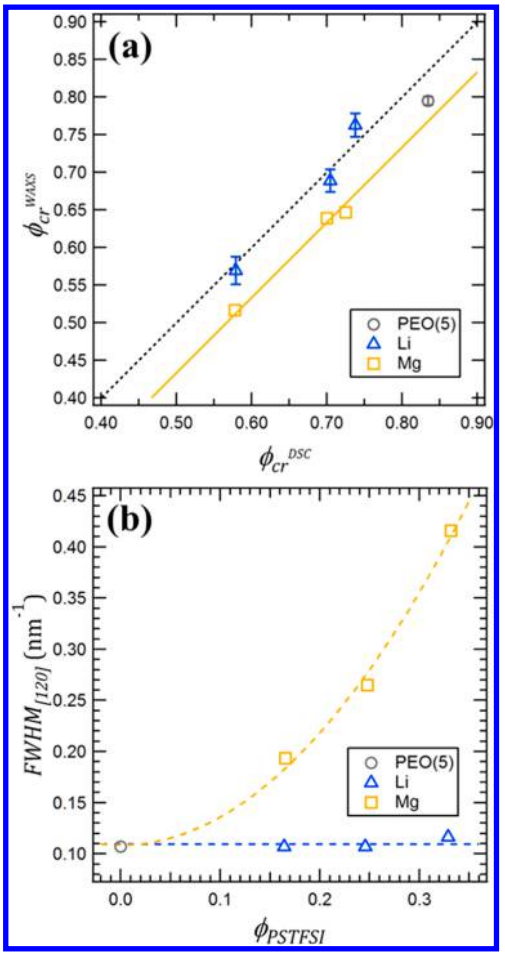

Figure 3. (a) Comparison of the fractional crystallinity of PEO determined through structural analysis (WAXS, ϕ_{cr}^{WAXS}) and thermal analysis (DSC, x_{cr}^{DSC}). Blue triangles indicate lithiated samples, gold squares indicate magnesiated samples, and gray circles indicate PEO(5). The error bars for PEO(5) and the lithiated samples indicate the range of values determined from different sector averages of the 2D WAXS data. The dashed black line indicates the prediction for a perfect correlation between ϕ_{cr}^{WAXS} and ϕ_{cr}^{DSC}, whereas the solid gold line represents a perfect correlation with a constant offset, determined by the best fit of a line with slope = 1 to the magnesiated data: $\phi_{cr}^{WAXS} = \phi_{cr}^{DSC} - 0.067(6)$. (b) Relationship between the full width at half-maximum of the PEO [120] scattering peak (fwhm$_{[120]}$) and the amount of P(STFSI) in the sample (ϕ_{PSTFSI}). Blue triangles indicate lithiated samples, gold squares indicate magnesiated samples, and the gray circle indicates PEO(5). The dashed lines are meant to guide the eye. The blue dashed line is the best fit to the lithiated and PEO(5) data with a slope set equal to zero: fwhm$_{[120]}$ = 0.110(2). The gold dashed line is the best fit of the magnesiated and PEO(5) data to a quadratic polynomial: fwhm$_{[120]}$ = 0.11(1) + 2.7(2)ϕ_{PSTFSI}^2. The fitting uncertainty in the last digit of each fit parameter is indicated by the value in parentheses.

chain crystals,[30] or it may demonstrate melting point depression due to the presence of dissociated ionic species.[14−17] If the PEO crystallizes into lamellae of the same thickness, L_{cryst}, for all samples (i.e., each PEO chain is folded the same number of times), then the simplest crystallization-induced nanostructure that could explain the SAXS profiles in Figure 2 would be stacked layers of crystalline PEO lamellae separated by an amorphous layer consisting of amorphous PEO and P(STFSI). In such a scenario, the interlamellar domain spacing (d_{SAXS}), which can be calculated from the position of

DOI: 10.1021/acs.macromol.7b00735
Macromolecules 2017, 50, 4827−4839

the primary SAXS scattering peak (q^*) by $d_{SAXS} = 2\pi/q^*$, should scale with the volume of amorphous material present in the sample. The volume of amorphous material can be calculated on a per-chain basis by the product $\phi_{am}V_{chain}$, where ϕ_{am} is total amorphous fraction in the sample and V_{chain} is the volume of an individual polymer chain. ϕ_{am} can be determined using knowledge of the sample composition and the PEO crystallinity through

$$\phi_{am} \equiv \phi_{PSTFSI} + \phi_{PEO}^{am} = \phi_{PSTFSI} + \phi_{PEO}[1 - \phi_{cr}] \quad (4)$$

where ϕ_{PEO}^{am} is the amorphous volume fraction of PEO within the semicrystalline sample and ϕ_{cr} is the crystalline volume fraction that can be obtained by either WAXS or DSC. The volume of an individual chain can be approximated by

$$V_{chain} = N_{PEO}v_{PEO} + N_{PSTFSI}v_{PSTFSI} \quad (5)$$

where N_{PEO} and N_{PSTFSI} are the degrees of polymerization for each block, and v_{PEO} and v_{PSTFSI} are their respective monomer volumes (v_{PEO} = 0.066 nm^3; v_{PSTFSI} = 0.34 nm^3).[5]

In Figure 4, we plot d_{SAXS} versus $\phi_{am}V_{chain}$ using the data from Figure 2 and Table 2. It is clear that the interlamellar

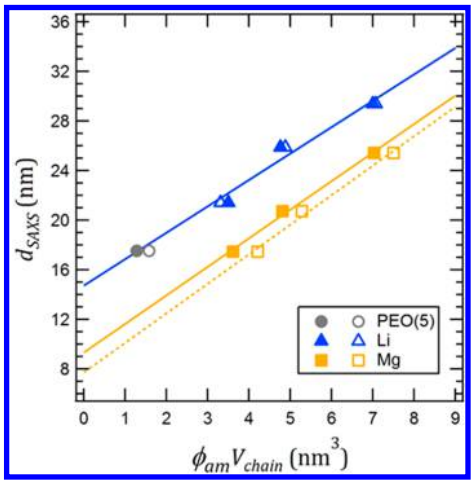

Figure 4. Relationship between nanostructure determined through SAXS and the fractional crystallinity of PEO. The lamellar spacing between PEO crystals (d_{SAXS}) is plotted versus the total amorphous volume contributed per chain ($\phi_{am}V_{chain}$). Blue triangles indicate lithiated samples, gold squares indicate magnesiated samples, and gray circles indicate PEO(5). Closed symbols use ϕ_{cr}^{DSC} to calculate ϕ_{am}, while open symbols use ϕ_{cr}^{WAXS}. The solid blue line represents the linear fit to the data from the lithiated polymers: d_{SAXS} = 2.1(2)$\phi_{am}V_{chain}$ + 15(1) (R^2 = 0.9598). The solid gold line represents the linear fit to the data from the magnesiated polymers using ϕ_{am} calculated from ϕ_{cr}^{DSC}: d_{SAXS} = 2.3(2)$\phi_{am}V_{chain}$ + 9.3(8) (R^2 = 0.9955), and the dashed gold line is the linear fit to the magnesiated polymers using ϕ_{am} calculated from ϕ_{cr}^{WAXS}: d_{SAXS} = 2.4(2)$\phi_{am}V_{chain}$ + 7.7(1.3) (R^2 = 0.9907). The fitting uncertainty in the last digit of each fit parameter is indicated by the value in parentheses.

domain spacing (d_{SAXS}) increases with increasing amorphous volume. If the PEO crystal thickness (L_{cryst}) remains constant between samples and nearly all chains participate in crystallization, then the interlamellar domain spacing can be expected to scale as

$$d_{SAXS} = \frac{\phi_{am}V_{chain}}{\alpha} + L_{cryst} \quad (6)$$

where α [nm^2] is the areal density of PEO−PSTFSI block junctions on the PEO crystal surface, which is fixed by the number of times the PEO chains fold within the crystal. We find that eq 6 accounts for the scaling behavior observed in all of the single-ion conducting block copolymers. In the case of the lithiated block copolymers, the scaling behavior falls in line with the data for PEO(5), and L_{cryst} = 15 ± 1 nm, as determined by the intercept of the linear fit shown in Figure 4. For a PEO sample with $M_{n,PEO}$ = 5 kg mol^{-1}, the thicknesses of crystalline lamellae comprising once- and twice-folded chains are 15.0 and 10.6 nm, respectively.[30] It appears that the PEO crystals in the lithiated polymer primarily comprise once-folded chains. The value of L_{cryst} for the lithiated samples also stands in good agreement with the width of the PEO-rich domains observed in the STEM image from PEO−P[(STFSI)Li](5-2.0) in Figure 2c. This indicates that a single once-folded PEO crystal spans the width of the PEO lamellar domain, i.e., the "homeotropic" crystal orientation.[32] The magnesiated block copolymers fall upon a separate line in Figure 4, with L_{cryst} = 9.3 ± 0.8 nm when using ϕ_{cr}^{DSC} to calculate ϕ_{am}(L_{cryst} = 7.7 ± 1.3 nm when using ϕ_{cr}^{WAXS} to calculate ϕ_{am}). The value of L_{cryst} determined from the magnesiated samples is roughly consistent with the thickness of PEO crystallites composed of twice-folded chains. However, since the melting temperatures between the lithiated and magnesiated matched pairs are similar, one might also expect a similar distribution of PEO crystals with once- and twice-folded chains. We posit that the consistently lower d_{SAXS} values in the magnesiated samples stems from a difference in nanostructure formation and crystal orientation (i.e., not "homeotropic"), rather than a significant difference in the population of PEO crystallite thicknesses.

It is known that the morphology of semicrystalline polymers is kinetically controlled.[7−10] Furthermore, it is known that polymer crystallization kinetics depend strongly on the degree of supercooling. Unlike the melting temperatures (T_m's), the crystallization temperatures (T_c's) observed in DSC (Table 2) are very different for the lithiated and magnesiated matched pairs, suggesting crystallization kinetics might differ considerably between samples, even under the same crystallization conditions. We probed the kinetics of PEO crystallization by quenching the block copolymers from temperatures well above the melting temperature of PEO to 35 °C and then monitoring the morphological development by *in situ* X-ray scattering. Time = 0 is defined as the time at which the sample temperature reached 35 °C (typically 45 min after the quench was initiated). In Figure 5a, we provide the combined SAXS/WAXS profiles for PEO−P[(STFSI)$_2$Mg](5-2.0) during such an experiment. We note that the SAXS and WAXS data were collected during two independent experiments; the absolute intensity data are simply plotted together to yield the profiles in Figure 5a. For time ≲30 min, the SAXS profile exhibits a single broad peak at q = 0.509 nm^{-1}. In this time window, the WAXS profile only contains intensity from the broad amorphous scattering halo.[27] While the SAXS profiles of molten P[(STFSI)$_2$Mg](5-2.0) (time <30 min) rule out the presence of ordered phases, the broad peak at q = 0.509 nm^{-1} can, in principle, arise from either highly disordered microphase separation or periodic concentration fluctuations. In ref 5, we showed that the SAXS profiles in the melt (time = 0 in Figure 5a) are consistent with the scattering from concentration fluctuations predicted by Leibler,[33] provided the Flory−Huggins interaction parameter and the statistical segment lengths of the chains are treated as adjustable parameters. For

DOI: 10.1021/acs.macromol.7b00735
Macromolecules 2017, 50, 4827−4839

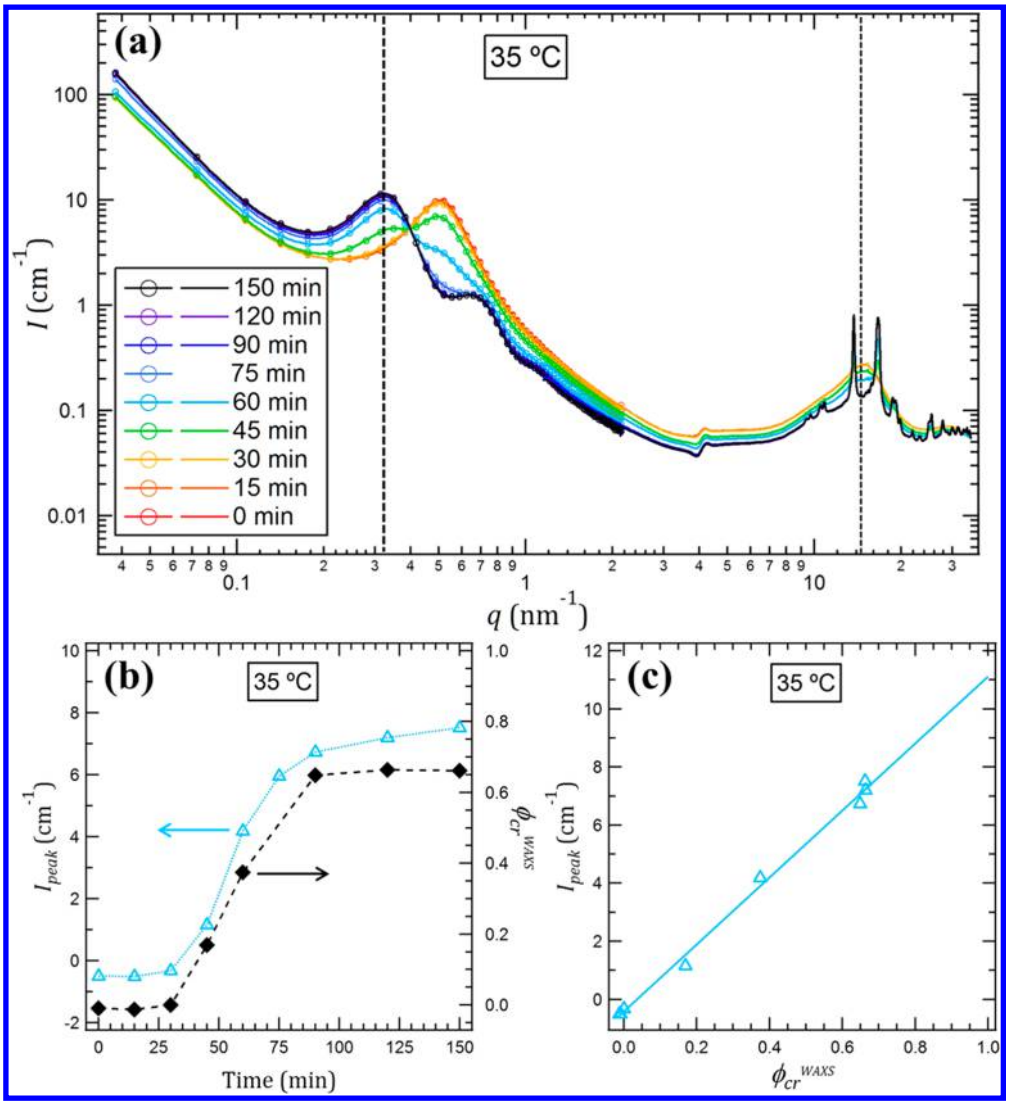

Figure 5. (a) Time-dependent combined SAXS/WAXS patterns from PEO−P[(STFSI)$_2$Mg](5-2.0) during isothermal crystallization at 35 °C. The dashed vertical lines indicate the q-values where intensities were extracted to calculate I_{peak} and ϕ_{cr}^{WAXS}. For clarity, the SAXS data markers are only plotted for every 15th data point and WAXS data are represented by lines between data points. (b) I_{peak} (left axis, open cyan triangles) and ϕ_{cr}^{WAXS} (right axis, filled black diamonds) plotted vs time during isothermal crystallization of PEO−P[(STFSI)$_2$Mg](5-2.0). Dashed curves are meant to guide the eye. (c) I_{peak} vs ϕ_{cr}^{WAXS} from the data shown in (b). The solid line indicates the linear fit to the data: $I_{peak} = 11.5(3)\phi_{cr}^{WAXS} - 0.4(1)$ (R^2 = 0.995).

simplicity, we refer to the structures obtained in molten P[(STFSI)$_2$Mg](5-2.0) as concentration fluctuations in the remainder of the paper.

Returning to Figure 5a, between time = 45 and 120 min, three changes occur in the scattering profile: the scattering peak from disordered fluctuations diminishes, a new scattering peak emerges at q = 0.325 nm^{-1}, and the WAXS intensity at q = 14.6 nm^{-1} decreases. The vertical dashed lines in Figure 5a are located at q = 0.325 and 14.6 nm^{-1}. The correlated changes in SAXS and WAXS at these two values of q are due to the formation of PEO-rich crystals. The Bragg peaks corresponding to PEO crystals are evident in the WAXS data obtained after time = 45 min. The formation of PEO crystals results in a dramatic increase in the length scale of the periodic structure from 12 to 19 nm. To our knowledge, such large changes in periodic length scale only occur within block copolymers during crystallization-induced self-assembly (e.g., unconfined or breakout crystallization).[6,8,9,34,35] It is perhaps worth noting that all of the scattering profiles in Figure 5a merge at q = 0.397 nm^{-1}. The scattering intensity at this value of q at time = 0 arises due to concentration fluctuations. Further work is needed to identify the reason why the scattering intensity from semicrystalline samples at this value of q is equal to that from amorphous fluctuations.

In Figure 5b, we quantify the correlation between SAXS and WAXS by plotting the normalized intensity (I_{peak}) of the primary SAXS peak (q^* = 0.325 nm^{-1}), calculated using eq 7, as well as the absolute PEO crystalline fraction (ϕ_{cr}^{WAXS}) versus time.

$$I_{peak} \equiv I_{35\ ^\circ C}(q^*) - I_{90\ ^\circ C}(q^*) \tag{7}$$

It is clear that I_{peak} and ϕ_{cr}^{WAXS} are correlated, which we demonstrate conclusively in Figure 5c by plotting I_{peak} versus ϕ_{cr}^{WAXS}. We note that I_{peak} reflects SAXS intensity at q = 0.325 nm^{-1}, while ϕ_{cr}^{WAXS} reflects WAXS intensity at q = 14.6 nm^{-1}. The linear relationship shown by the regression analysis in Figure 5c indicates that I_{peak} is a measure of relative crystallinity.

DOI: 10.1021/acs.macromol.7b00735
Macromolecules 2017, 50, 4827−4839

In Figure 6, we show time-dependent SAXS profiles for PEO−P[(STFSI)Li](5-3.2) after quenching from 70 to 35 °C.

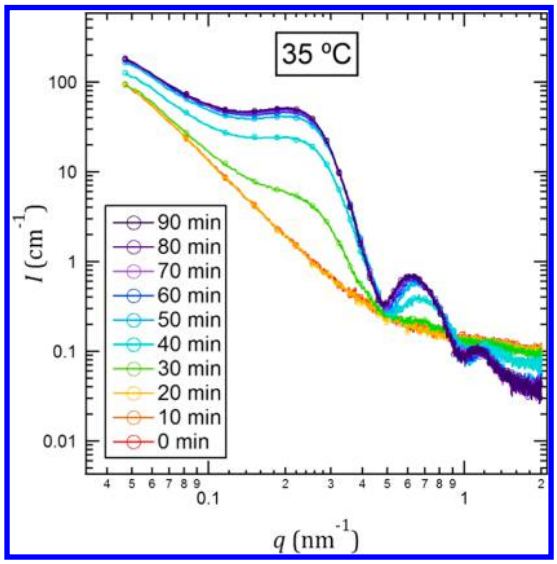

Figure 6. Time-dependent *in situ* SAXS profiles from PEO−P[(STFSI)Li](5-3.2) during isothermal crystallization at 35 °C.

We see the development of crystalline lamellae, indicated by the growth of a peak at q = 0.215 nm^{-1}. The main difference between the lithiated sample in Figure 6 and magnesiated sample in Figure 5 is the absence of the broad scattering peak due to concentration fluctuations in the fully amorphous state (compare time = 0 data in Figures 5a and 6). We note that we were unable to replicate the experiment with PEO−P[(STFSI)-Li](5-3.2) using a WAXS configuration due to limited access to the beamline.

The *in situ* SAXS experiments described above were performed on all of the single-ion conducting block copolymers. (The *in situ* SAXS profiles from samples not shown in Figures 5 and 6 are provided in the Supporting Information (SI 5)). In Figure 7, we plot I_{peak} extracted from all of the samples versus time. In Figure 7a, we show that PEO−P[(STFSI)Li](5-1.1) and PEO−P[(STFSI)Li](5-2.0) are essentially fully crystallized by the time the *in situ* SAXS heating stage reached 35 °C. This result is consistent with DSC observations showing T_c ∼ 35 °C for those samples. Interestingly, PEO−P[(STFSI)Li](5-3.2), which did not portray a detectable crystallization temperature during the DSC cooling scan (see Table 2), began to rapidly crystallize 20 min after the stage reached the 35 °C set point. The crystallization time for PEO−P[(STFSI)Li](5-3.2), approximated using the linear fits in Figure 7a, was 53 min. The cooling rate employed in the DSC experiments precluded crystallization in this sample. It is evident in Figure 7a that the rate of crystallization decreases as the molecular weight of the P[(STFSI)Li] block is increased from 1.1 to 3.2 kg mol^{-1}. In Figure 7b, we show the time dependence of I_{peak} of the magnesiated block copolymers. In this set, the rate of crystallization also decreases with increasing molecular weight of the P(STFSI) block. Crystallization of PEO−P-[(STFSI)$_2$Mg](5-1.1) is essentially complete at time = 0. With a crystallization time of ∼71 min, the crystallization of PEO−P[(STFSI)$_2$Mg](5-2.0) is qualitatively similar to PEO−P[(STFSI)Li](5-3.2). The crystallization of PEO−P-[(STFSI)$_2$Mg](5-3.2) is very slow and was not observed over

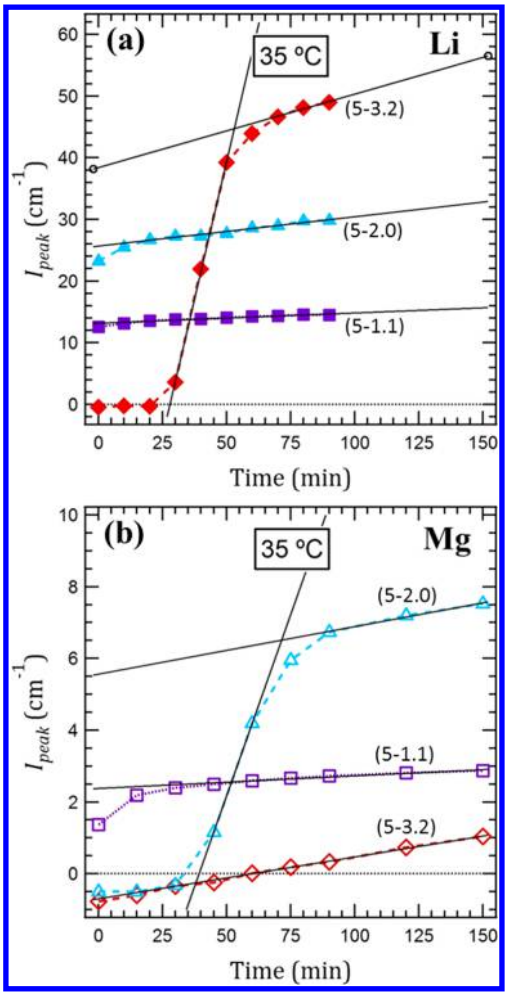

Figure 7. Evolution of the semicrystalline SAXS peak intensity (I_{peak}) with time during isothermal crystallization at 35 °C for (a) the lithiated samples (closed symbols) and (b) the magnesiated samples (open symbols). Red diamonds = PEO−P(STFSI)(5-3.2); cyan triangles = PEO−P(STFSI)(5-2.0); purple squares = PEO−P(STFSI)-(5-1.1). The dashed curves are meant to guide the eye. The black lines were used to approximate the crystallization times for each sample.

the course of the experiment; note that I_{peak} only increases by 2 cm^{-1} during the experiment (Figure 7b) (negative values of I_{peak} can be obtained because of our definition (eq 7)). WAXS data obtained at time = 150 min for PEO−P[(STFSI)$_2$Mg](5-3.2) showed no evidence of PEO Bragg peaks (SI 5). The rate of crystallization in the magnesiated samples as measured by SAXS is reflective of their crystallization temperatures observed by DSC. Table 3 summarizes the approximate crystallization times determined by *in situ* SAXS for each set of matched pairs.

The time-dependent data in Figures 5−7 represent three different states: (1) a homogeneous disordered state in the lithiated samples at early times, (2) a disordered state with

Table 3. Crystallization Times (in min) at 35 °C[a]

matched pair	Li	Mg
PEO−P(STFSI)(5-3.2)	∼53	>150
PEO−P(STFSI)(5-2.0)	<10	∼71
PEO−P(STFSI)(5-1.1)	∼0	<15

[a]Based on the data in Figure 7; a time of ∼0 indicates crystallization occurred at T > 35 °C during the quench.

DOI: 10.1021/acs.macromol.7b00735
Macromolecules 2017, 50, 4827−4839

concentration fluctuations in the magnesiated samples at early times, and (3) lamellar microphases induced by PEO crystallization in both samples at late times. We posit that the differences in crystallization kinetics observed between matched pairs of lithiated and magnesiated single-ion conducting block copolymers stem from differences in their melt morphology. Before crystallization, the SAXS profile from the magnesiated sample (PEO−P[(STFSI)$_2$Mg](5-2.0)) indicates the presence of periodic concentration fluctuations, whereas the SAXS profile from lithiated sample (PEO−P[(STFSI)Li](5-3.2)) is essentially featureless and does not indicate the presence of periodic fluctuations. To characterize the different states within these samples, we turn to the SAXS invariant (Q). Q provides a measure of the magnitude of electron density fluctuations within a sample and is related to the difference in scattering length densities of the two polymer blocks.[36] The SAXS invariant is defined as

$$Q = \frac{1}{2\pi^2}\int_{q_{min}}^{q_{max}} I(q)q^2\,dq \quad \text{cm}^{-1}\,\text{nm}^{-3} \tag{8}$$

In principle, the integration limits should be $q_{min} = 0$ and $q_{max} = \infty$; however, in practice, the extrapolations of $I(q)$ to $q = 0$ and $q = \infty$ lead to significant errors in the calculation of Q.[27,36] We set the integration bounds based on the experimentally measured SAXS q-range (q_{min} = 0.04 nm^{-1} and q_{max} = 2.0 nm^{-1}) and used the NCNR Analysis Macro[37] package for Igor Pro to calculate the invariant; no fluctuating background intensity was subtracted from the SAXS curves prior to integration.[38] In Figure 8, we plot Q versus time during the isothermal crystallization of PEO−P[(STFSI)Li](5-3.2) and PEO−P[(STFSI)$_2$Mg](5-2.0), the two samples wherein crystallization kinetics occurred on accessible time scales. The trends observed in these two samples are qualitatively different, with Q increasing for the lithiated PEO−P[(STFSI)Li](5-3.2) sample and Q decreasing for the magnesiated PEO−P[(STFSI)$_2$Mg](5-2.0) sample as the PEO chains crystallize. Furthermore, the absolute values of Q in the fully molten state (i.e., at time = 0) for PEO−P[(STFSI)$_2$Mg](5-2.0) is nearly 4 times greater than that of PEO−P[(STFSI)Li](5-3.2). We first analyze the discrepancy in values of Q in the molten state and then propose a pathway that can explain the opposing trends in Q during crystallization.

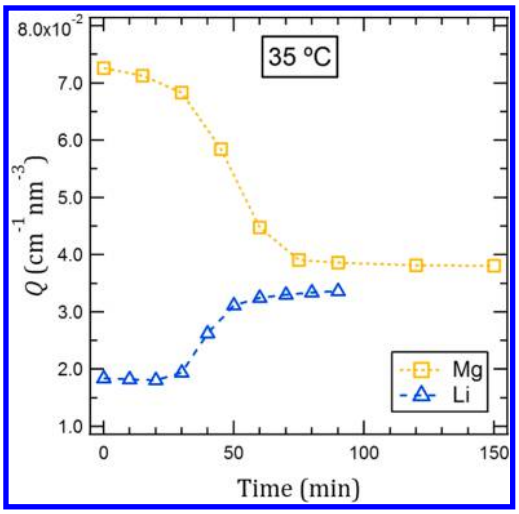

Figure 8. Evolution of the SAXS invariant (Q) during the isothermal crystallization of PEO−P[(STFSI)Li](5-3.2) (blue triangles) and PEO−P[(STFSI)$_2$Mg](5-2.0) (gold squares) at 35 °C. Dashed curves are meant to guide the eye.

In an ideal two-phase system with sharp interfaces, the SAXS invariant (Q_{ideal}) is determined by the volume fraction of each phase and their scattering contrast:

$$Q_{ideal} = 1 \times 10^{-21}(B_A - B_B)^2\phi_A\phi_B \quad \text{cm}^{-1}\,\text{nm}^{-3} \tag{9}$$

where B_A and B_B are the scattering length densities and ϕ_A and ϕ_B are the volume fractions of phases A and B. The factor of 1×10^{-21} is a simple unit conversion factor required to convert the $(B_A - B_B)^2$ cm^{-4} term into the appropriate units. The phases of interest here are PEO and the PSTFSI. In Table 4, we provide the values of $1 \times 10^{-21}(B_A - B_B)^2$ and $\phi_A\phi_B$, which are calculated as described previously,[5] for PEO−P[(STFSI)$_2$Mg](5-2.0) and PEO−P[(STFSI)Li](5-3.2) at 35 °C. We provide these calculations under two conditions: first assuming fully amorphous PEO (ρ_{am}^{PEO} = 1.112 g cm^{-3})[22] and second assuming 100% crystalline PEO (ρ_{cr}^{PEO} = 1.24 g cm^{-3}).[27] In both cases we use a density for the P(STFSI) block of ρ_{PSTFSI} = 1.57 g cm^{-3}.[4] (We have not explicitly measured the density of P-[(STFSI)$_2$Mg] and assume that it is the same as P[(STFSI)Li]. Given the fact that the monomers are bulky and mostly organic in nature (see Figure 1), we expect this assumption to hold.) The changes in Q_{ideal} during crystallization can be estimated using the data in Table 4. For both the lithiated and magnesiaed samples, Q_{ideal} is predicted to decrease by a factor of about 2 upon PEO crystallization. The magnesitated sample (PEO−P[(STFSI)$_2$Mg](5-2.0)) follows this behavior, with Q decreasing from 0.073 to 0.038 cm^{-1} nm^{-3} upon crystallization. This result suggests the presence of large amplitude concentration fluctuations in PEO−P[(STFSI)$_2$Mg](5-2.0). The presence of such fluctuations in short disordered block copolymers has been established both theoretically and experimentally.[39,40] In contrast, the increase in Q seen in the lithiated PEO−P[(STFSI)Li](5-3.2) sample during crystallization cannot be explained by the ideal two-phase model.

For a two-phase system with diffuse interface boundaries, the relation for the ideal SAXS invariant (Q_{ideal}) in eq 9 must be modified. By using a three-dimensional Gaussian smoothing function, the SAXS invariant for a two-phase system with diffuse interfaces (Q_{diff}) can be written as

Table 4. Calculated Values Relating Q_{ideal} Assuming Fully Amorphous PEO and 100% Crystalline PEO in the PEO−P[(STFSI)Li](5-3.2) and PEO−P[(STFSI)2Mg](5-2.0) Samples

	amorphous PEO		100% crystalline PEO	
sample	$1 \times 10^{-21}(B_A - B_B)^2$ [cm^{-1} nm^{-3}]	$\phi_A\phi_B$	$1 \times 10^{-21}(B_A - B_B)^2$ [cm^{-1} nm^{-3}]	$\phi_A\phi_B$
PEO−P[(STFSI)$_2$Mg](5−2.0)	1.11	0.19	0.46	0.20
PEO−P[(STFSI)Li](5−3.2)	1.06	0.22	0.43	0.23

DOI: 10.1021/acs.macromol.7b00735
Macromolecules 2017, 50, 4827−4839

$$Q_{diff} = 1 \times 10^{-21}(B_A - B_B)^2 \phi_A \phi_B \left(1 - \frac{t}{l_p}\right) \quad (10)$$

where t is the thickness of the interface region and l_p is Porod's length of inhomogeneity, which describes the average "domain size" within the sample.[36] In Table 5, we provide the measured

Table 5. Invariant Values and Diffuse Interface Thicknesses[a]

sample	Q [cm^{-1} nm^{-3}]	Q_{ideal} [cm^{-1} nm^{-3}]	t/l_p
PEO−P[(STFSI)$_2$Mg](5-2.0) at time = 0	0.073	0.21	0.65
PEO−P[(STFSI)Li](5-3.2) at time = 0	0.018	0.24	0.92
PEO−P[(STFSI)$_2$Mg](5-2.0) at time = 150	0.038	0.09	0.58
PEO−P[(STFSI)Li](5-3.2) at time = 90	0.033	0.10	0.66

[a]Experimental (Q) and ideal (Q_{ideal}) invariant values for PEO−P[(STFSI)Li](5-3.2) and PEO−P[(STFSI)$_2$Mg](5-2.0) at the beginning and end of the *in situ* SAXS experiments. t/l_p values are the results from eq 11.

SAXS invariants (Q) for the magnesiated PEO−P[(STFSI)$_2$Mg](5-2.0) and lithiated PEO−P[(STFSI)Li](5-3.2) samples before and after PEO crystallization, along with the corresponding calculated values of Q_{ideal} for those samples in the fully amorphous and 100% crystalline state, respectively. In the final column of Table 5, we provide the value of t/l_p necessary to yield the experimentally measured invariant values assuming a diffuse interface, which we calculate using Q and Q_{ideal} in eq 11:

$$\frac{t}{l_p} = 1 - \frac{Q}{Q_{ideal}} \quad (11)$$

It is clear from Table 5 that, in the melt, the thickness (t) of the diffuse interface layer (relative to the "domain size" (l_p)) is much larger for the lithiated sample. In fact, the value of t/l_p = 0.92 indicates that "domains" in PEO−P[(STFSI)Li](5-3.2) are extremely diffuse. We conclude that the increase in Q during crystallization in PEO−P[(STFSI)Li](5-3.2) arises from the formation of new interface boundaries as PEO crystallites form within the homogeneous PEO−P[(STFSI)Li] melt. In contrast, the value of t/l_p = 0.65 calculated for PEO−P[(STFSI)$_2$Mg](5-2.0) in the melt is similar to the value determined for the semicrystalline PEO−P[(STFSI)Li](5-3.2) sample (t/l_p = 0.66), indicating that the phase boundaries that form upon crystallization are just as diffuse as the dynamic interfaces that are present in the molten state with concentration fluctuations. We note in passing determining absolute values of interfacial thickness accurately is difficult. Clearly, using the same model to quantify three dramatically different states, a homogeneous disordered state, a disordered state with fluctuations, and a semicrystalline ordered state may be thought of as a crude first step toward the characterization of crystallization in single-ion conducting block copolymers. The values for t/l_p provided in Table 5 represent an upper bound for (t), since the measured SAXS invariant (Q) used in eq 11 is determined from the experimentally limited region of q-space. Furthermore, our treatment of the invariant in this work is derived for a two-phase system, and strictly speaking, the semicrystalline samples might need to be treated as three-phase systems; however, the qualitative interpretation of our results should still hold. Extension of our treatment to three-phase systems is outside the scope of this paper.

In Figure 9, we provide schematics of the nanostructures of molten and semicrystalline PEO−P[(STFSI)$_2$Mg] and PEO−P[(STFSI)Li] that are consistent with the structural insights from the static SAXS/WAXS and STEM measurements in Figure 2 as well as with the *in situ* scattering data from Figures 5 and 6. In Figure 9a, we demonstrate periodic concentration fluctuations in the PEO−P[(STFSI)$_2$Mg] melt, whereas PEO−P[(STFSI)Li] is homogeneous in the melt. Upon crystallization, the periodicity of the fluctuations in PEO−P[(STFSI)$_2$Mg] increases by nearly a factor of 2, consistent with the *in situ* SAXS profiles from the PEO−P[(STFSI)$_2$Mg]-

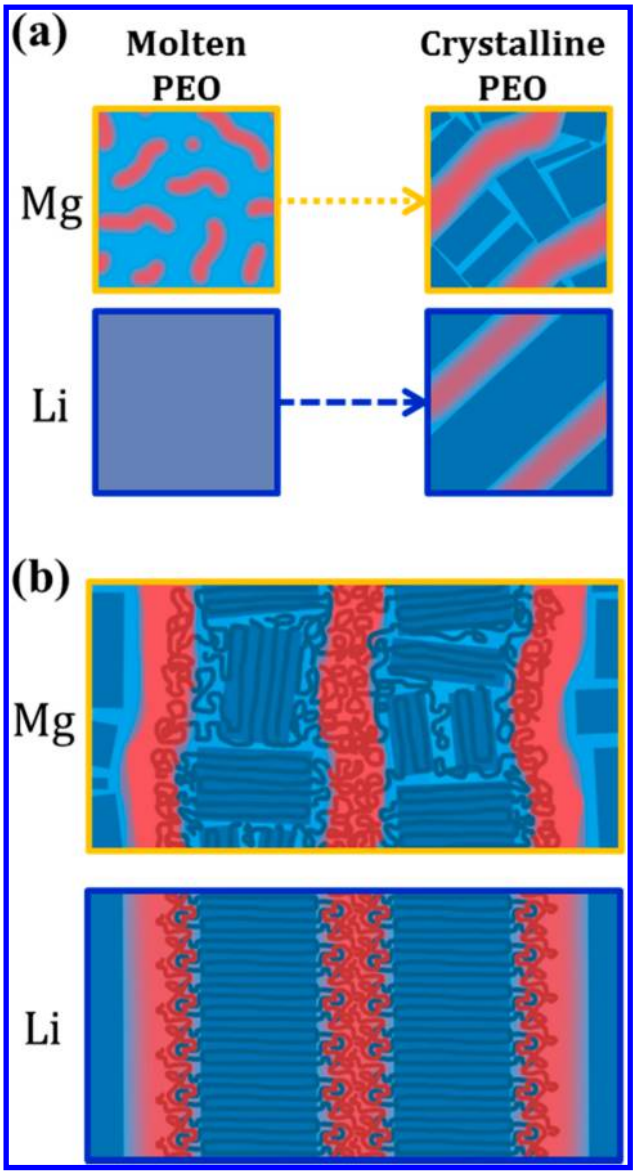

Figure 9. (a) Cartoons depicting possible composition profiles and (b) chain configurations that could lead to the observed invariants as well as the scattering profiles in Figures 4 and 5. The cartoons highlighted in gold represent PEO−P[(STFSI)$_2$Mg], and the cartoons highlighted with blue represent PEO−P[(STFSI)Li]. Red indicates P(STFSI), cyan indicates amorphous PEO, blue parallelograms indicate crystalline PEO, and violet indicates well-mixed PEO and P(STFSI).

DOI: 10.1021/acs.macromol.7b00735
Macromolecules 2017, 50, 4827−4839

(5-2.0) sample. We believe the rearrangement of the P[(STFSI)$_2$Mg]-rich regions required for this change in periodicity causes the slower crystallization kinetics and increased disorder observed in the magnesiated samples. In other words, PEO crystallization in the magnesiated samples is disrupted by the presence of the disordered P[(STFSI)$_2$Mg]-rich concentration fluctuations. In contrast, crystallization in PEO−P[(STFSI)Li] leads to the formation of periodic structure from the homogeneous melt, as revealed by an increase in the scattering invariant upon crystallization and the formation of peaks in the SAXS profiles in Figure 6. In Figure 9b, we demonstrate possible chain configurations that could lead to the semicrystalline structures depicted in Figure 9a; crystallite orientation in the magnesiated sample is depicted as random, whereas the crystallites in the lithiated sample are depicted in the "homeotropic" orientation.[32]

CONCLUSION

Single-ion conducting block copolymers composed of the ion-containing block poly(styrene-4-sulfonyltrifluoromethylsulfonyl)imide (P(STFSI)) and the ion solvating/conducting block poly(ethylene oxide) (PEO) represent a unique class of materials, wherein single-ion conduction occurs by solvating and transporting the cation with the neutral polymer block (PEO).[2−4] In this study we report on the crystallization behavior of PEO within a matched pair library of lithiated (PEO−P[(STFSI)Li]) and magnesiated (PEO−P[(STFSI)$_2$Mg]) single-ion conducting block copolymers. DSC analysis revealed that the P(STFSI) counterion (Li^+ or Mg^{2+}) does not significantly affect PEO crystallinity. SAXS/WAXS and STEM analysis revealed that PEO crystallization induces the formation of lamellar morphologies in all samples; however, the magnesiated samples were found to have increased levels of disorder at both crystalline and nanostructural length scales.

We studied the kinetics of PEO crystallization in the matched pairs using the absolute scattering intensity data from independent time-resolved *in situ* SAXS and WAXS experiments. These experiments show that PEO crystallization is significantly slowed when the P(STFSI) counterion is switched from Li^+ to Mg^{2+}. In the molten state, the lithiated samples are homogeneous, whereas the magnesiated samples contain concentration fluctuations. The homogeneous nature of the lithiated samples allows PEO to crystallize into well-ordered lamellae, similar to those observed in homopolymer PEO(5). We attribute the slowed crystallization kinetics as well as the increased structural disorder observed in the semicrystalline magnesiated samples to the presence of concentration fluctuations in the melt. Thus, the identity of the P(STFSI) counterion (Li^+ vs Mg^{2+}), which dictates the interactions between P(STFSI) and PEO in the melt state,[5] ultimately controls the kinetics of PEO crystallization and the formation of concomitant crystallization-induced nanostructure.

ASSOCIATED CONTENT

Supporting Information

The Supporting Information is available free of charge on the ACS Publications website at DOI: 10.1021/acs.macromol.7b00735.

SI 1: differential scanning calorimetry (DSC) data and analysis from the single-ion conducting block copolymers and PEO(5); SI 2: details about the SAXS/WAXS setup and data reduction procedure; SI 3: a detailed derivation of the angle-dependent absorbance correction applied to the WAXS data, as well the procedure used to calibrate scattering intensities to absolute units; SI 4: details regarding the quantitative analysis of the SAXS/WAXS data, including a derivation of our recast Goppel approximation for determining absolute crystallinity from WAXS of block copolymers with one crystallizable block; SI 5: all of the scattering data collected in this study along with the results from the peak fitting described in SI 4 and the values extracted from the WAXS data that were used to calculate PEO crystallinity (PDF)

AUTHOR INFORMATION

Corresponding Author

*E-mail: nbalsara@berkeley.edu (N.P.B.).

ORCID

Jacob L. Thelen: 0000-0003-0026-4404

Nitash P. Balsara: 0000-0002-0106-5565

Notes

The authors declare no competing financial interest.

ACKNOWLEDGMENTS

This work was supported by the Joint Center for Energy Storage Research, an Energy Innovation Hub funded by the U.S. Department of Energy (DOE), Office of Science, Basic Energy Sciences (BES). DSC measurements were performed at the Molecular Foundry at Lawrence Berkeley National Laboratory. STEM measurements were performed at the National Center for Electron Microscopy, which is also part of the Molecular Foundry. X-ray scattering experiments were performed at Lawrence Berkeley National Laboratory's Advance Light Source, Beamline 7.3.3. The Molecular Foundry and Beamline 7.3.3 of the Advanced Light Source are supported by the Director of the Office of Science, Office of Basic Energy Sciences, of the U.S. Department of Energy under Contract DE-AC02-05CH11231. We thank Polite Stewart, Chenhui Zhu, and Eric Schaible for their assistance with the setup and operation of Beamline 7.3.3.

NOMENCLATURE

Abbreviations

AgB	silver behenate
DSC	differential scanning calorimetry
PEO	poly(ethylene oxide)
PEO-*b*-P[STFSI]	poly(ethylene oxide)-*b*-poly[(styrene-4-sulfonyltrifluoromethylsulfonyl)-imide] diblock copolymer, unspecified ion
PEO−P[(STFSI)Li]	poly(ethylene oxide)-*b*-poly[(styrene-4-sulfonyltrifluoromethylsulfonyl)-imide lithium]
PEO−P[(STFSI)$_2$Mg]	poly(ethylene oxide)-*b*-poly[(styrene-4-sulfonyltrifluoromethylsulfonyl)-imide magnesium]
P(STFSI)	poly[(styrene-4-sulfonyltrifluoromethylsulfonyl)imide], unspecified ion
PS	polystyrene
S−D	sample-to-detector distance
SAXS	small-angle X-ray scattering

DOI: 10.1021/acs.macromol.7b00735
Macromolecules 2017, 50, 4827−4839

STEM	scanning transmission electron microscopy
WAXS	wide-angle X-ray scattering

Symbols

d_{SAXS}	interlamellar domain spacing, nm
$fwhm_{[120]}$	full width at half-maximum of the [120] WAXS peak, nm^{-1}
ΔH_m	experimentally measured specific melting enthalpy, J g^{-1}
ΔH_m°	ideal specific melting enthalpy, J g^{-1}
I	scattering intensity, cm^{-1}
$I_{p,[120]}$	fit parameter corresponding to the [120] WAXS peak height, cm^{-1}
I_{peak}	intensity at $q = q^*$, normalized by the molten sample intensity, cm^{-1}
L_{cryst}	crystal lamellae thickness, nm
l_p	Porod's length of inhomogeneity, nm
$M_{n,PEO}$	number-average molecular weight of PEO block, kg mol^{-1}
$M_{n,PSTFSI}$	number-average molecular weight of P(STFSI) block, kg mol^{-1}
N_{PEO}	number-average degree of polymerization of PEO block
N_{PSTFSI}	number-average degree of polymerization of P(STFSI) block
q	magnitude of the scattering vector, nm^{-1}
q^*	position of the primary SAXS peak, nm^{-1}
$q_{p,[120]}$	the fitted [120] WAXS peak position, nm^{-1}
q_0	location where I_{scr} and I_{molten} are evaluated to calculate ϕ_{cr}^{WAXS}, nm^{-1}
Q	SAXS scattering invariant, cm^{-1}
Q_{diff}	scattering invariant for two-phase system with diffuse interfaces, cm^{-1}
Q_{ideal}	ideal scattering invariant for two-phase system, cm^{-1}
q_{max}	maximum attainable scattering vector in SAXS, nm^{-1}
q_{min}	minimum attainable scattering vector in SAXS, nm^{-1}
t	domain interface thickness, nm
T_c	crystallization temperature, °C
T_g	glass transition temperature, °C
T_m	melting temperature, °C
v_{PEO}	monomer volume for EO, nm^3
v_{PSTFSI}	monomer volume for STFSI, nm^3
V_{chain}	volume of a single chain, nm^3
w_{PEO}	weight fraction of PEO
x_{cr}^{DSC}	mass fractional crystallinity calculated through DSC

Greeks

α	areal density of block junctions on the PEO crystal surface, nm^{-2}
χ	Flory–Huggins interaction parameter
ϕ_{am}^{scr}	amorphous volume fraction of a semi crystalline polymer block
ϕ_{am}	total amorphous volume fraction within a semi crystalline polymer
ϕ_{cr}^{DSC}	volume fractional crystallinity calculated through DSC
ϕ_{cr}^{WAXS}	volume fractional crystallinity calculated through WAXS
ϕ_{PEO}	volume fraction of the PEO block
ϕ_{PSTFSI}	volume fraction of the P(STFSI) block
λ	scattering wavelength, nm
ρ_{am}^{PEO}	density of amorphous poly(ethylene oxide), g cm^{-3}
ρ_{cr}^{PEO}	density of crystalline poly(ethylene oxide), g cm^{-3}
ρ_{PSTFSI}	density of poly[(styrene-4-sulfonyltrifluoromethylsulfonyl)imide], g cm^{-3}
θ	scattering angle, rad

REFERENCES

(1) Ryu, S.-W.; Trapa, P. E.; Olugebefola, S. C.; Gonzalez-Leon, J. A.; Sadoway, D. R.; Mayes, A. M. Effect of Counter Ion Placement on Conductivity in Single-Ion Conducting Block Copolymer Electrolytes. *J. Electrochem. Soc.* **2005**, *152*, A158.

(2) Bouchet, R.; Maria, S.; Meziane, R.; Aboulaich, A.; Lienafa, L.; Bonnet, J.; Phan, T. N. T.; Bertin, D.; Gigmes, D.; Devaux, D.; et al. Single-Ion BAB Triblock Copolymers as Highly Efficient Electrolytes for Lithium-Metal Batteries. *Nat. Mater.* **2013**, *12*, 452–457.

(3) Inceoglu, S.; Rojas, A. A.; Devaux, D.; Chen, X. C.; Stone, G. M.; Balsara, N. P. Morphology–Conductivity Relationship of Single-Ion-Conducting Block Copolymer Electrolytes for Lithium Batteries. *ACS Macro Lett.* **2014**, *3*, 510–514.

(4) Rojas, A. A.; Inceoglu, S.; Mackay, N. G.; Thelen, J. L.; Devaux, D.; Stone, G. M.; Balsara, N. P. Effect of Lithium-Ion Concentration on Morphology and Ion Transport in Single-Ion-Conducting Block Copolymer Electrolytes. *Macromolecules* **2015**, *48*, 6589–6595.

(5) Thelen, J. L.; Inceoglu, S.; Venkatesan, N. R.; Mackay, N. G.; Balsara, N. P. Relationship between Ion Dissociation, Melt Morphology, and Electrochemical Performance of Lithium and Magnesium Single-Ion Conducting Block Copolymers. *Macromolecules* **2016**, *49*, 9139–9147.

(6) Loo, Y. L.; Register, R. A.; Ryan, A. J. Modes of Crystallization in Block Copolymer Microdomains: Breakout, Templated, and Confined. *Macromolecules* **2002**, *35*, 2365–2374.

(7) He, W. N.; Xu, J. T. Crystallization Assisted Self-Assembly of Semicrystalline Block Copolymers. *Prog. Polym. Sci.* **2012**, *37*, 1350–1400.

(8) Quiram, D. J.; Register, R. A.; Marchand, G. R.; Ryan, A. J. Dynamics of Structure Formation and Crystallization in Asymmetric Diblock Copolymers. *Macromolecules* **1997**, *30*, 8338–8343.

(9) Zhu, L.; Chen, Y.; Zhang, A.; Calhoun, B.; Chun, M.; Quirk, R.; Cheng, S.; Hsiao, B.; Yeh, F.; Hashimoto, T. Phase Structures and Morphologies Determined by Competitions among Self-Organization, Crystallization, and Vitrification in a Disordered Poly(ethylene Oxide)-B-Polystyrene Diblock Copolymer. *Phys. Rev. B: Condens. Matter Mater. Phys.* **1999**, *60*, 10022–10031.

(10) Ryan, A. J.; Hamley, I. W.; Bras, W.; Bates, F. S. Structure Development in Semicrystalline Diblock Copolymers Crystallizing from the Ordered Melt. *Macromolecules* **1995**, *28*, 3860–3868.

(11) Huang, P.; Zhu, L.; Guo, Y.; Ge, Q.; Jing, A. J.; Chen, W. Y.; Quirk, R. P.; Cheng, S. Z. D.; Thomas, E. L.; Lotz, B.; et al. Confinement Size Effect on Crystal Orientation Changes of Poly(ethylene Oxide) Blocks in Poly(ethylene Oxide)- B -Polystyrene Diblock Copolymers. *Macromolecules* **2004**, *37*, 3689–3698.

(12) Huang, P.; Guo, Y.; Quirk, R. P.; Ruan, J.; Lotz, B.; Thomas, E. L.; Hsiao, B. S.; Avila-Orta, C. A.; Sics, I.; Cheng, S. Z. D. Comparison of Poly(ethylene Oxide) Crystal Orientations and Crystallization Behaviors in Nano-Confined Cylinders Constructed by a Poly(ethylene Oxide)-B-Polystyrene Diblock Copolymer and a Blend of Poly(ethylene Oxide)-B-Polystyrene and Polystyrene. *Polymer* **2006**, *47*, 5457–5466.

(13) Zhu, L.; Cheng, S. Z. D.; Calhoun, B. H.; Ge, Q.; Quirk, R. P.; Thomas, E. L.; Hsiao, B. S.; Yeh, F.; Lotz, B. Phase Structures and Morphologies Determined by Self-Organization, Vitrification, and Crystallization: Confined Crystallization in an Ordered Lamellar Phase of PEO-B-PS Diblock Copolymer. *Polymer* **2001**, *42*, 5829–5839.

(14) Lascaud, S.; Perrier, M.; Vallee, A.; Besner, S.; Prud'homme, J.; Armand, M. Phase Diagrams and Conductivity Behavior of Poly(ethylene Oxide)-Molten Salt Rubbery Electrolytes. *Macromolecules* **1994**, *27*, 7469–7477.

(15) Moulin, J.-F.; Damman, P.; Dosière, M. Poly(ethylene Oxide)/lithium Triflate Phase Diagram. *Polymer* **1999**, *40*, 5843–5850.

DOI: 10.1021/acs.macromol.7b00735
Macromolecules 2017, 50, 4827–4839

(16) Vallée, A.; Besner, S.; Prud'Homme, J. Comparative Study of Poly(ethylene Oxide) Electrolytes Made with LiN(CF3SO2)2, LiCF3SO3 and LiClO4: Thermal Properties and Conductivity Behaviour. *Electrochim. Acta* **1992**, *37*, 1579−1583.
(17) Chintapalli, M.; Le, T. N. P.; Venkatesan, N. R.; Mackay, N. G.; Rojas, A. A.; Thelen, J. L.; Chen, X. C.; Devaux, D.; Balsara, N. P. Structure and Ionic Conductivity of Polystyrene- *Block* -Poly(ethylene Oxide) Electrolytes in the High Salt Concentration Limit. *Macromolecules* **2016**, *49*, 1770−1780.
(18) Hexemer, A.; Bras, W.; Glossinger, J.; Schaible, E.; Gann, E.; Kirian, R.; MacDowell, A.; Church, M.; Rude, B.; Padmore, H. A SAXS/WAXS/GISAXS Beamline with Multilayer Monochromator. *J. Phys. Conf. Ser.* **2010**, *247*, 012007.
(19) Ilavsky, J. Nika: Software for Two-Dimensional Data Reduction. *J. Appl. Crystallogr.* **2012**, *45*, 324−328.
(20) Zhang, F.; Ilavsky, J.; Long, G. G.; Quintana, J. P. G.; Allen, A. J.; Jemian, P. R. Glassy Carbon as an Absolute Intensity Calibration Standard for Small-Angle Scattering. *Metall. Mater. Trans. A* **2010**, *41*, 1151−1158.
(21) Wang, W.; Liu, W.; Tudryn, G. J.; Colby, R. H.; Winey, K. I. Multi-Length Scale Morphology of Poly(ethylene Oxide)-Based Sulfonate Ionomers with Alkali Cations at Room Temperature. *Macromolecules* **2010**, *43*, 4223−4229.
(22) *Physical Properties of Polymers Handbook*; Mark, J. E., Ed.; Springer: New York, 2007.
(23) Beaumont, R. H.; Clegg, B.; Gee, G.; Herbert, J. B. M.; Marks, D. J.; Roberts, R. C.; Sims, D. Heat Capacities of Propylene Oxide and of Some Polymers of Ethylene and Propylene Oxides. *Polymer* **1966**, *7*, 401−417.
(24) Afifi-Effat, A. M.; Hay, J. N. Enthalpy and Entropy of Fusion and the Equilibrium Melting Point of Polyethylene Oxide. *J. Chem. Soc., Faraday Trans. 2* **1972**, *68*, 656.
(25) Ruland, W. X-Ray Determination of Crystallinity and Diffuse Disorder Scattering. *Acta Crystallogr.* **1961**, *14*, 1180−1185.
(26) Polizzi, S.; Fagherazzi, G.; Benedetti, A.; Battagliarin, M.; Asano, T. A Fitting Method for the Determination of Crystallinity by Means of X-Ray Diffraction. *J. Appl. Crystallogr.* **1990**, *23*, 359−365.
(27) Alexander, L. E. *X-Ray Diffraction Methods in Polymer Science*; Wiley-Interscience: New York, 1969.
(28) Balko, J.; Lohwasser, R. H.; Sommer, M.; Thelakkat, M.; Thurn-Albrecht, T. Determination of the Crystallinity of Semicrystalline Poly(3-Hexylthiophene) by Means of Wide-Angle X-Ray Scattering. *Macromolecules* **2013**, *46*, 9642−9651.
(29) Crist, B.; Cohen, J. B. Fourier Analysis of Polymer X-Ray Diffraction Patterns. *J. Polym. Sci., Polym. Phys. Ed.* **1979**, *17*, 1001−1010.
(30) Kovacs, A. J.; Straupe, C.; Gonthier, A. Isothermal Growth, Thickening, and Melting of Polyethylene Oxide) Single Crystals in the Bulk. II. *J. Polym. Sci., Polym. Symp.* **1977**, *59*, 31−54.
(31) Kovacs, A. J.; Gonthier, A.; Straupe, C. Isothermal Growth, Thickening, and Melting of Poly(ethylene Oxide) Single Crystals in the Bulk. *J. Polym. Sci., Polym. Symp.* **1975**, *50*, 283−325.
(32) Zhu, L.; Cheng, S. Z. D.; Calhoun, B. H.; Ge, Q.; Quirk, R. P.; Thomas, E. L.; Hsiao, B. S.; Yeh, F.; Lotz, B. Crystallization Temperature-Dependent Crystal Orientations within Nanoscale Confined Lamellae of a Self-Assembled Crystalline - Amorphous Diblock Copolymer. *J. Am. Chem. Soc.* **2000**, *122*, 5957−5967.
(33) Leibler, L. Theory of Microphase Separation in Block Copolymers. *Macromolecules* **1980**, *13*, 1602−1617.
(34) Rangarajan, P.; Register, R. A.; Fetters, L. J.; Bras, W.; Naylor, S.; Ryan, A. J. Crystallization of a Weakly Segregated Polyolefin Diblock Copolymer. *Macromolecules* **1995**, *28*, 4932−4938.
(35) Nojima, S.; Kato, K.; Yamamoto, S.; Ashida, T. Crystallization of Block Copolymers. 1. Small-Angle X-Ray Scattering Study of a.epsilon.-Caprolactone-Butadiene Diblock Copolymer. *Macromolecules* **1992**, *25*, 2237−2242.
(36) Roe, R.-J. *Methods of X-Ray and Nuetron Scattering in Polymer Science*; Oxford University Press Inc.: 2000.
(37) Kline, S. R. Reduction and Analysis of SANS and USANS Data Using IGOR Pro. *J. Appl. Crystallogr.* **2006**, *39*, 895−900.
(38) Vonk, C. G. Investigation of Non-Ideal Two-Phase Polymer Structures by Small-Angle X-Ray Scattering. *J. Appl. Crystallogr.* **1973**, *6*, 81−86.
(39) Fredrickson, G. H.; Helfand, E. Fluctuation Effects in the Theory of Microphase Separation in Block Copolymers. *J. Chem. Phys.* **1987**, *87*, 697.
(40) Rosedale, J. H.; Bates, F. S.; Almdal, K.; Mortensen, K.; Wignall, G. D. Order and Disorder in Symmetric Diblock Copolymer Melts. *Macromolecules* **1995**, *28*, 1429−1443.

DOI: 10.1021/acs.macromol.7b00735
Macromolecules 2017, 50, 4827−4839